INTERNATIONAL JOURNAL FOR NUMERICAL METHODS IN FLUIDS
Int. J. Numer. Meth. Fluids 2000; **33**: 1099–1119

The steady annular extrusion of a Newtonian liquid under gravity and surface tension

Kostas Housiadas[a], Georgios Georgiou[b,*,1] and John Tsamopoulos[a]

[a] *Department of Chemical Engineering, University of Patras, Patras, Greece*
[b] *Department of Mathematics and Statistics, University of Cyprus, Nicosia, Cyprus*

SUMMARY

The steady extrusion of a Newtonian liquid through an annular die and its development outside and away from the die are studied under the influence of gravitational and surface tension forces. The finite element method (FEM) is used for the simulations. The positions of the inner and outer free surface profiles are calculated simultaneously with the other unknown fields, i.e. using the Newton–Raphson iterative scheme. The effects of three relevant parameters, i.e. the Reynolds, the Stokes and the capillary numbers, on the shape of the annular film are studied for two values of the inner to the outer diameter ratio, corresponding to a thick and a thin annular film respectively. A one-dimensional model for the extrudate region, valid for thin annular films, is also presented, and its predictions are compared with the two-dimensional finite element calculations. Despite the fact that it is valid away from the die exit, the one-dimensional model predicts satisfactorily the effects of the Stokes and capillary numbers. Copyright © 2000 John Wiley & Sons, Ltd.

KEY WORDS: annular flow; extrudate swell; finite elements; thin film approximation

1. INTRODUCTION

Steady extrusion through annular dies has application in the manufacturing of pipes and is closely related to the film blowing and wire coating processes. As in extrusion through slits and capillaries, the amount of change in the extrudate size (swelling) is a very important design parameter, since accurate dimensions of the extruded products are required. Hence, the simulation of the annular extrusion process has been the subject of quite a few publications in the past two decades [1–6]. To our knowledge, in all two-dimensional studies of annular extrusion reported so far, gravity and surface tension are neglected, which is not the case in simulations of extrusion through slits and dies [7–11]. However, it is known from experimental

* Correspondence to: Department of Mathematics and Statistics, University of Cyprus, PO Box 20537, 1678 Nicosia, Cyprus. Tel.: + 357 2 892208; fax: + 357 2 339061.
[1] E-mail: georgios@ucy.ac.cy

Received 24 May 1999
Revised 11 October 1999

observations that both gravity and surface tension push the annular film towards the axis of symmetry and have a dramatic effect on the shape of the extrudate. When surface tension is high, the extruded annular film closes, forming a jet at a distance from the exit, known as the *closing length* [12]. The latter decreases with surface tension.

In the early 1980s, Crochet and Keunings [1] used finite elements to solve the annular flow of an upper-convected Maxwell fluid at zero Reynolds number, zero gravity and zero surface tension, with the ratio of inner to outer diameter equal to 0.75. They calculated the unknown positions of the free surfaces iteratively using a Picard-iteration technique (i.e. a successive substitution scheme). Mitsoulis [2] solved the creeping annular flow of a Newtonian fluid using a similar method and studied the effect of the diameter ratio. Mitsoulis and Heng [3] studied numerically the isothermal extrusion of different fluids through annular dies. Ahn and Ryan [4] used finite differences to solve the non-isothermal annular extrusion of a Newtonian fluid. Huynh [5] solved the non-isothermal extrusion of Newtonian fluids through annular dies using finite elements and Picard iterations. He studied, in particular, the influence of temperature and die gap size on the extrudate's swelling behaviour. Numerical simulations for viscoelastic annular swell flow have been carried out by various groups (see Reference [6] and references therein).

The effects of surface tension and gravity have been taken into account in theoretical one-dimensional analyses, used to model the unsteady flow of thin annular and slender cylindrical or planar films (see References [13–15] and references therein). In the first case, the thickness of the film is small compared with the inner radius of the annulus; in the second one, the thickness of the film is small compared with its length. One-dimensional models are produced (i) by using *ad hoc* balances on the film [16], (ii) by simplifying the two-dimensional equations using a perturbation expansion in the film slenderness [17], or (iii) by employing a co-ordinate system that moves with the film and writing directly the one-dimensional momentum and mass balances that are valid in the thin film limit [18]. The resulting equations are clearly simpler, since the dependence of all variables on the co-ordinate normal to the film axis is eliminated. On the other hand, one-dimensional models are not valid inside and near the extruder, where the flow is inherently two-dimensional, and their validity away from the extruder can only be ascertained if either the next order problem in the perturbation expansion or the corresponding two-dimensional problem is solved.

The main objective of this paper is to solve numerically the two-dimensional, steady Newtonian annular extrusion flow, and study the effects of gravity and surface tension forces on the shape of the extrudate. It is assumed that the closing length is large, i.e. the jet closes far downstream from the exit plane of the computational domain. It is also assumed that the pressures inside and outside the annular jet are equal. As a consequence, the jet shape can be considered to have reached an asymptote and the axial velocity can be assumed to be almost uniform at the exit plane. In such a case, the normal component of the traction is vanishing at the exit plane. Similar assumptions for the velocity and the normal traction at the exit plane have been made in various theoretical and numerical studies of both the axisymmetric and planar extrudate swell problems under gravity and surface tension, and are valid when the exit plane is taken sufficiently far from the exit of the die [7–11]. In the numerical simulations, we use the finite element method (FEM) with the Newton–Raphson iterative scheme for the calculation of the unknown positions of the inner and outer free surfaces, i.e. the positions of the two surfaces are calculated simultaneously with the other unknown fields [9].

Another objective of this work is to compare the two-dimensional calculations with the predictions of the steady state counterpart of the theoretical one-dimensional model of Housiadas and Tsamopoulos [13–15], developed for unsteady thin annular films. Obviously, a fair comparison between the two models can only be made after taking into account that the control volume of the one-dimensional model starts away from the exit of the die, where the flow ceases to be two-dimensional. This requires the detailed study of the domain of validity of the one-dimensional model in terms of the four dimensionless parameters involved, i.e. the Reynolds, the Stokes and the capillary numbers and the diameter ratio. Such a study might prove useful in developing a hybrid simulation package involving two-dimensional modelling of the flow inside the annulus and in the rearrangement zone of the extrudate, and one-dimensional modelling away from the die exit. Although this combination would optimize the accuracy and speed of the numerical calculations, it is not attempted here because it would introduce, as an additional parameter, the location where the patching between the two models takes place. In this study, it has been chosen, instead, to start the one-dimensional calculations at the point where the two-dimensional model predicts a maximum for the outer free surface.

The rest of the paper is organized as follows. In Section 2, the governing equations and the boundary conditions for the two-dimensional flow are presented, and the FEM used in the simulations is briefly discussed. In Section 3, the basic equations of the one-dimensional model are given, and the method of solution is briefly described. In Section 4, the numerical results are discussed. Two-dimensional results are presented for various values of the Reynolds, Stokes and capillary numbers and two values of the diameter ratio corresponding to a thick and a thin film respectively. The predictions of the one-dimensional model for the latter case are in fairly good agreement with the two-dimensional results. The conclusions are summarized in Section 5.

2. TWO-DIMENSIONAL ANALYSIS

The flow geometry and the governing equations of the annular extrusion are depicted in Figure 1(a). The flow is assumed to be isothermal and axisymmetric. The fluid is incompressible and has constant viscosity μ. Cylindrical co-ordinates are employed with the z-axis coinciding with the axis of symmetry of the flow. To non-dimensionalize the governing equations, we use as a scaling parameter for lengths the inner radius R_{in} of the annulus; the velocity vector $\mathbf{v}$ is scaled by the average velocity U in the annulus; and finally, the pressure p and the stress tensor $\boldsymbol{\tau}$ are measured in units of $\mu U/R_{\text{in}}$. Thus, the dimensionless steady state continuity and momentum equations read

$$\nabla\cdot\mathbf{v} = 0 \tag{1}$$

$$Re\,\mathbf{v}\cdot\nabla\mathbf{v} = -\nabla p - \nabla\cdot\boldsymbol{\tau} + St\,\mathbf{e}_z \tag{2}$$

where

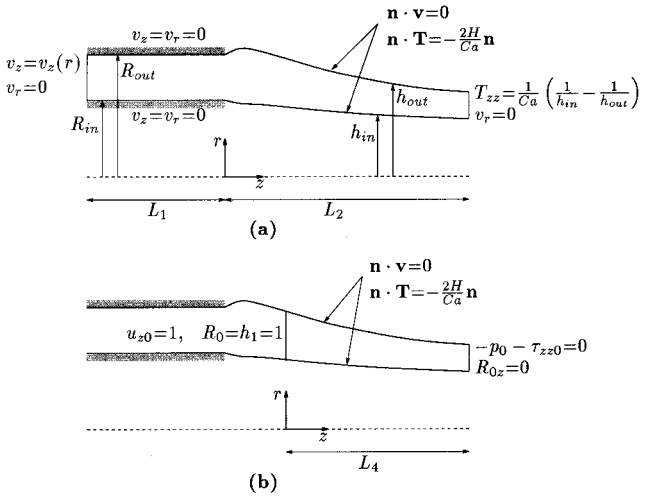

Figure 1. Geometry and boundary conditions of the annular extrusion flow: (a) two-dimensional model, (b) one-dimensional model.

$$Re \equiv \frac{\rho U R_{\text{in}}}{\mu} \tag{3}$$

and

$$St \equiv \frac{\rho g R_{\text{in}}^2}{\mu U} \tag{4}$$

are the Reynolds and Stokes numbers respectively, ρ is the density, g is the gravitational acceleration and $\mathbf{e}_z$ denotes the unit vector in the axial direction.

In addition to the two velocity components, v_z and v_r, and the pressure p, the positions h_{in} and h_{out} of the inner and outer free surfaces of the extrudate are additional unknowns in the annular extrusion problem. The kinematic condition that the free surfaces remain material surfaces provides the additional equation needed

$$\mathbf{n} \cdot \mathbf{v} = 0 \tag{5}$$

where $\mathbf{n}$ is the unit normal vector pointing outwards from a free surface.

The remaining two conditions on the free surface serve as the boundary conditions in the formulation. A momentum balance on the free surface requires the shear stress to vanish and the normal stress in the liquid to balance any capillary pressure. If

$$\mathbf{T} = -p\mathbf{I} - \boldsymbol{\tau} \tag{6}$$

is the total stress tensor, **I** being the unit tensor, then

$$\mathbf{n}\cdot\mathbf{T} = -\frac{2H}{Ca}\,\mathbf{n} \tag{7}$$

Ca is the capillary number, defined by

$$Ca \equiv \frac{\mu U}{\sigma} \tag{8}$$

where σ is the surface tension and $2H$ is the mean curvature of a free surface, given by

$$-2H = \frac{h_{zz}}{[1+h_z^2]^{3/2}} - \frac{1}{h\sqrt{1+h_z^2}} \tag{9}$$

Note that the subscripts z and zz denote first- and second-order differentiation of h with respect to z.

As for the remaining boundary conditions, standard assumptions are made. Along the solid walls both the velocity components vanish. At the inlet plane, taken at a distance L_1 upstream the die exit, the flow is assumed to be fully developed, i.e. v_r is zero and v_z is given by the standard solution for Poiseuille flow in an annulus. Finally, at the outlet plane, taken at a distance L_2 downstream from the die exit, the flow is assumed to be approximately uniform, and thus

$$-p - \tau_{zz} = \frac{1}{Ca}\left(\frac{1}{h_{\text{in}}} - \frac{1}{h_{\text{out}}}\right) \quad \text{and} \quad v_r = 0 \tag{10}$$

where τ_{zz} is the normal stress component. (Note that the subscript zz denotes here the zz-component of the stress tensor $\boldsymbol{\tau}$.) As discussed in Section 4, these outflow boundary conditions lead to satisfactory results up to $z = L_2/4$, provided that L_2 is sufficiently large.

The two-dimensional flow problem has been solved using finite elements. The flow domain is discretized by means of quadrilateral elements. The velocity components and the pressure are approximated by means of biquadratic and bilinear shape functions respectively. The unknown positions, h_{in} and h_{out}, of the two surfaces of the annular extrudate are approximated by means of quadratic shape functions. The standard Galerkin method is used to weight the momentum and the continuity equations over the flow domain, and the kinematic equation on the two free surfaces. The resulting non-linear system of equations is solved using the Newton method and a standard frontal sub-routine. The mesh is updated at each iteration according to the newly found positions of the inner and outer free surfaces using the spine technique [9].

In order to study the convergence of the numerical solution and investigate the validity of the boundary condition at the exit plane, we constructed meshes of different refinement and of different lengths. All the meshes extended up to $L_1 = 5\epsilon$ upstream, where

$$\epsilon \equiv \frac{R_{out} - R_{in}}{R_{in}} = \frac{R_{out}}{R_{in}} - 1 \tag{11}$$

In order to determine the appropriate length L_2 of the domain downstream of the exit, we considered nine different values ranging from 20ϵ to 6400ϵ. In Table I, we tabulate useful data about the meshes used for the case $\epsilon = 0.5$. Note that meshes more refined than those of Table I have also been used. In Figure 2, we show part of mesh 9, which requires the simultaneous solution of 36855 equations. A typical run with this mesh requires about 15 min of CPU time on an IBM AIX RISC 6000 workstation.

Table I. Data for meshes used for the case $\epsilon = 0.5$.

Mesh	L_2/ϵ	Number of elements	Number of unknowns
1	20	710	6957
2	50	950	9333
3	100	1540	15 174
4	200	2330	22 995
5	400	2610	25 767
6	800	2890	28 539
7	1600	3170	31 311
8	3200	3450	34 083
9	6400	3730	36 855

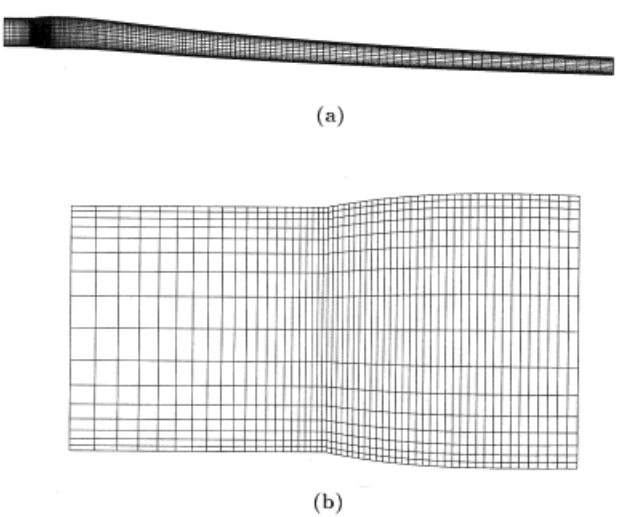

Figure 2. (a) Part of mesh 9 used for $\epsilon = 0.5$; (b) enlargement near the die exit.

3. ONE-DIMENSIONAL ANALYSIS

The procedure we have chosen for producing the one-dimensional model starts by writing the complete two-dimensional equations in a fixed cylindrical co-ordinate system and the conditions at the four parts of the boundary, i.e. the two unknown free surfaces, the inlet plane at $z = 0$ (i.e. at a distance $L_2 - L_4$ from the exit), assumed to be so far away from the exit of the die so that the one-dimensional model is valid, and the outlet plane taken further downstream, at $z = L_4$.

It is noted here that, in the one-dimensional analysis, the co-ordinate system is shifted downstream from the die exit. Moreover, since the one-dimensional model does not involve the die region (see Figure 1(b)), the ratio ϵ is redefined as follows:

$$\epsilon \equiv \left. \frac{h_{\text{out}} - h_{\text{in}}}{h_{\text{in}}} \right|_{z=0} \tag{12}$$

The dimensionless numbers have to be redefined as well. For example, the Reynolds and Stokes numbers are now given by

$$Re \equiv \frac{\rho U h_{\text{in}}|_{z=0}}{\mu} \tag{13}$$

and

$$St \equiv \frac{\rho g h_{\text{in}}^2|_{z=0}}{\mu U} \tag{14}$$

where U is now the average axial velocity at $z = 0$. It is clear that this average velocity is different from the average velocity inside the die, used in non-dimensionalizing the two-dimensional equations. Owing to the acceleration of the film caused by gravity, the former is expected to be higher.

The next step is to map the unknown free surfaces onto fixed ones by means of a non-orthogonal mapping, as explained in Reference [13]. The dependent variables of the problem are the two velocity components, v_z and v_r, the pressure p, the inner film radius h_{in}, and the thickness Δh of the film

$$\Delta h \equiv h_{\text{out}} - h_{\text{in}} \tag{15}$$

We employ a regular perturbation scheme for the dependent variables, with ϵ as the perturbation parameter. Owing to the definition of ϵ, the thickness Δh of the film has no zero-order contribution. The peculiarity of this problem is that in order to formally obtain a complete set of the lowest-order governing equations and boundary conditions, one needs to combine perturbation equations from up to three different orders of magnitude [13,17,19]

$$\begin{bmatrix} v_z \\ v_r \\ p \\ h_{\text{in}} \\ \Delta h \end{bmatrix} = \begin{bmatrix} v_{z0} \\ v_{r0} \\ p_0 \\ R_0 \\ 0 \end{bmatrix} + \epsilon \begin{bmatrix} v_{z1} \\ v_{r1} \\ p_1 \\ R_1 \\ h_1 \end{bmatrix} + \epsilon^2 \begin{bmatrix} v_{z2} \\ v_{r2} \\ p_2 \\ R_2 \\ h_2 \end{bmatrix} + O(\epsilon^3) \tag{16}$$

which obviously is valid only for small values of ϵ. The subscripts 0, 1 and 2 in the right-hand side of Equation (16) denote the zero-, first- and second-order contributions to the corresponding dependent variables.

The final equations are ordinary differential equations in the axial direction only, with the axial velocity v_{z0} and the inner radius R_0 as unknowns. The thickness of the film (i.e. h_1) is eliminated from the momentum balances by combining the mass conservation of the film at $O(\epsilon^0)$ with the difference of the kinematic conditions at $O(\epsilon^1)$ to get

$$h_1 R_0 v_{z0} = 1 \tag{17}$$

The steps for deriving the governing equation are briefly given in the following. After imposing the normal force boundary condition (7) at $O(\epsilon^1)$, the momentum balance in the direction normal to the inner surface of the film at $O(\epsilon^0)$ becomes

$$\frac{\tau_{rr0} - \tau_{\phi\phi 0}}{R_0} + (p_0 + \tau_{zz0})\left(R_{0zz} - \frac{R_{0z}^2}{R_0}\right) + St\, R_{0z} + Re\, v_{z0}^2 R_{0zz} + \frac{2}{h_1 Ca'}(2H)_0 = 0 \tag{18}$$

where

$$Ca' \equiv \frac{Ca}{\epsilon} \tag{19}$$

This new definition of the capillary number is necessary, because in the process of deriving Equation (18), one finds that the thin film cannot sustain a large capillary force [13,19,20].

Similarly, the tangential to the inner film surface momentum balance at $O(\epsilon^0)$ with the zero tangential stress boundary condition at $O(\epsilon^1)$gives

$$\begin{aligned} &- St + (1 + R_{0z}^2)\frac{\mathrm{d}(p_0 + \tau_{zz0})}{\mathrm{d}z} + (p_0 + \tau_{zz0})\left[R_{0z}\left(\frac{1}{R_0} + R_{0zz}\right) + \frac{h_{1z}}{h_1}(1 + R_{0z}^2)\right] \\ &+ \frac{R_{0z}(\tau_{rr0} - \tau_{\phi\phi 0})}{R_0} + Re\left[v_{z0}^2 R_{0z} R_{0zz} + (1 + R_{0z}^2) v_{z0}\frac{\mathrm{d}v_{z0}}{\mathrm{d}z}\right] = 0 \end{aligned} \tag{20}$$

Note that the radial velocity v_{r0} has been eliminated from Equations (18) and (20) by means of

$$v_{r0} = v_{z0} R_{0z} \tag{21}$$

This equation is obtained by combining the continuity equation at $O(\epsilon^1)$and the kinematic condition at the two free surfaces at $O(\epsilon^0)$; for more details see Reference [13]. As for the pressure p_0, this is calculated from the normal stress balance at the free surfaces at $O(\epsilon^0)$

$$p_0 = \frac{-\tau_{rr0} + 2R_{0z}\tau_{rz0} - R_{0z}^2\tau_{zz0}}{1 + R_{0z}^2} \tag{22}$$

In Equations (18) and (20), the following symbols have been used:

$$h_{1z} \equiv \frac{\mathrm{d}h_1}{\mathrm{d}z}, \qquad R_{0z} \equiv \frac{\mathrm{d}R_0}{\mathrm{d}z} \quad \text{and} \quad R_{0zz} \equiv \frac{\mathrm{d}^2R_0}{\mathrm{d}z^2} \tag{23}$$

Therefore, the mean curvature at zero-order is

$$(2H)_0 = \frac{\sqrt{1 + R_{0z}^2}}{R_0} - \frac{R_{0zz}}{\sqrt{1 + R_{0z}^2}}$$

Moreover, for the components of the stress tensor, we have

$$\tau_{rr0} = -2S_{r1} \tag{24}$$

$$\tau_{zz0} = -2\left(\frac{\mathrm{d}v_{z0}}{\mathrm{d}z} - R_{0z}S_{z1}\right) \tag{25}$$

$$\tau_{rz0} = -\frac{\mathrm{d}v_{z0}}{\mathrm{d}z} + R_{0z}S_{r1} - S_{z1} \tag{26}$$

$$\tau_{\phi\phi0} = -\frac{2v_{r0}}{R_0} \tag{27}$$

where S_{z1} and S_{r1} are the derivatives of v_{z1} and v_{r1} respectively with respect to r

$$S_{z1} \equiv \frac{1}{h_1}\frac{\partial v_{z1}}{\partial r} = \frac{1}{1 + R_{0z}^2}\left[R_{0z}\left(\frac{v_{r0}}{R_0} + \frac{\mathrm{d}v_{z0}}{\mathrm{d}z}\right) + \frac{1}{1 + R_{0z}^2}\left(2R_{0z}\frac{\mathrm{d}v_{z0}}{\mathrm{d}z} - \frac{\mathrm{d}v_{r0}}{\mathrm{d}z}(1 - R_{0z}^2)\right)\right] \tag{28}$$

$$S_{r1} \equiv \frac{1}{h_1}\frac{\partial v_{r1}}{\partial r} = R_{0z}S_{z1} - \frac{\mathrm{d}v_{z0}}{\mathrm{d}z} - \frac{v_{r0}}{R_0} \tag{29}$$

The expressions for S_{z1} and S_{r1} were derived by combining the tangential stress conditions at $O(\epsilon^0)$ with the indentity

$$\tau_{rr0} + \tau_{\phi\phi0} + \tau_{zz0} = 0 \tag{30}$$

The boundary conditions at the planes $z = 0$ and L_4 are imposed in an average sense [17], but at this order of approximation of the thin film, they reduce to

$$\text{At } z = 0, \quad v_{z0} = 1, \quad R_0 = 1 \quad \text{and} \quad h_1 = 1 \tag{31}$$

$$\text{At } z = L_4, \quad -p_0 - \tau_{zz0} = 0 \quad \text{and} \quad R_{0z} = 0 \tag{32}$$

Note that the second condition at $z = L_4$ is equivalent to $v_{r0} = 0$, as easily deduced from Equation (21).

For convenience with the finite element solution and for increased accuracy, R_{0z} is treated as an additional dependent variable [13]. It is calculated by solving its defining equation

$$\frac{dR_0}{dz} = R_{0z} \tag{33}$$

After combining the above equations in order to eliminate all variables except for R_0, R_{0z} and u_{z0}, Equations (18), (20) and (33) are solved numerically using the Galerkin–FEM. Quadratic, isoparametric Lagrangian basis functions are employed for the three dependent variables. The nodes were introduced at the following locations:

$$z_i = L_4\left(\frac{i-1}{n}\right)^a, \quad i = 1, 2, \ldots, n \tag{34}$$

where n is the total number of nodes and the exponent a was chosen to be $a = 2.2$ in order to concentrate the nodes near the inlet plane. Convergence of the numerical results was checked by using meshes with different values of n. The effect of the length of the domain was checked by considering two different lengths, $L_4 = 3200\epsilon$ and 6400ϵ. In order to achieve four accurate digits in the axial velocity and the inner surface of the film, 120 elements were used in the most demanding case, where $St = 1$ and $L_4 = 6400\epsilon$. This resulted in 723 unknowns to be calculated. These requirements become less restrictive as the dimensionless numbers decrease. In most cases, 80 elements are sufficient. The computational time in a Pentium II running at 90 MHz is only 2–6 s of CPU time.

4. RESULTS AND DISCUSSION

We have considered two values of the ratio ϵ, i.e. $\epsilon = 0.5$ and 0.1, corresponding to a 'thick' and a 'thin' annular film respectively. For the case $\epsilon = 0.5$, only two-dimensional calculations will be presented. We first studied the creeping flow ($Re = 0$) with zero surface tension ($Ca = \infty$ and various Stokes numbers, and obtained results with meshes of different length L_2. In Figure 3, we show results for $St = 0.04$, illustrating the effect of L_2 on the numerical solution. The value $L_2 = 400$ is more than adequate for accurately capturing the solution in the region up to $z = 50$. Indeed, in most cases examined, it was found that calculations with film lengths equal to L_2 provided film shapes that were independent of this length up to a distance $z \sim L_2/4$. Thus, although gravity constantly applies an axial force on the film, one may apply the simpler boundary condition given by Equation (10) at some finite length and still get converged shapes for 20–25 per cent of this film length.

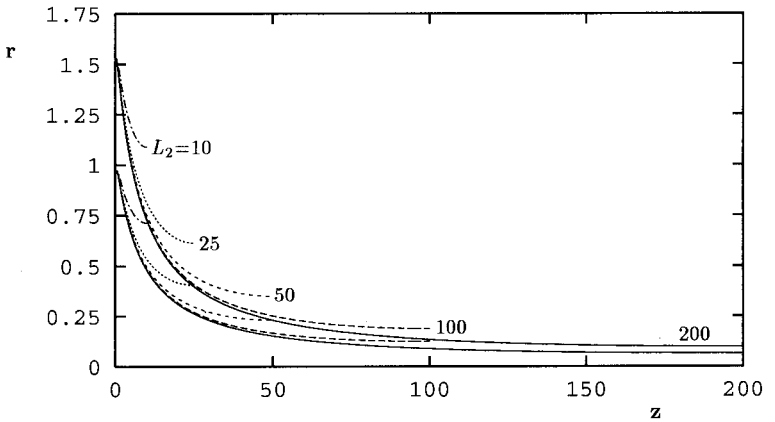

Figure 3. Convergence of the solution with L_2; $St = 0.04$, $\epsilon = 0.5$, $Re = 0$ and $Ca = \infty$.

In Figure 4, the effect of the Stokes number on the shape of the annular extrudate is illustrated. Here it is concluded again that converged shapes up to $z = 50$ are obtained using $L_2 = 200$, since no significant deviation is observed when $L_2 = 400$. Owing to its annular shape and finite thickness, the film swells near the die exit in a non-symmetric way. The rapid variation in its thickness lasts for less than 3 per cent of its length shown in Figure 4. This first region of the film is followed by a second much larger one without any swelling. Here, gravity forces the film inwards and the film becomes thinner due to the acceleration of the fluid. Note that if the axial velocity remained constant while the film was pushed towards the symmetry axis, its thickness would have to increase owing to the conservation of mass.

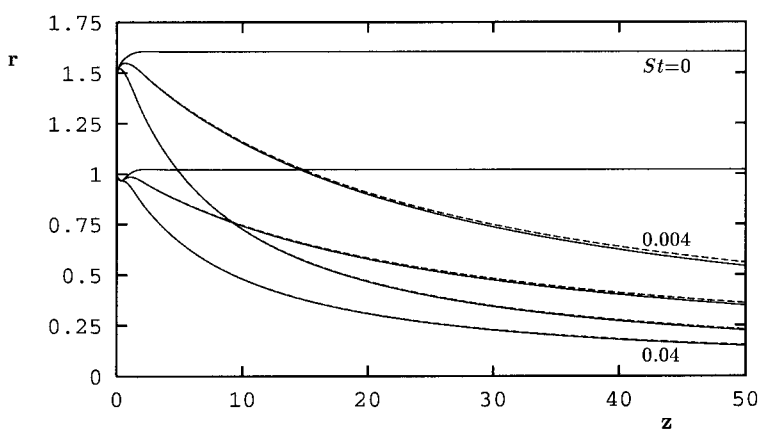

Figure 4. Annular extrudates for various Stokes numbers, $\epsilon = 0.5$, $Re = 0$ and $Ca = \infty$, obtained with $L_2 = 400$ (solid lines) and 200 (dashed lines).

The above observation explains also the results of Figure 5, where we illustrate the effect of Ca on the annular films for $Re = 0$ and $St = 0$. Surface tension forces the annular film towards the axis of symmetry; since the volumetric flow rate is constant and no axial acceleration is applied, the thickness of the film increases with the axial distance. The inner surface is thus bound to reach the axis of symmetry at a critical distance L_3 downstream (the closing length). Therefore, when Ca is low (i.e. the surface tension is high), our annular flow formulation is not valid for long solution domains. The closing length L_3 is reduced as Ca decreases. Obviously, in the case of zero Re and St, we are unable to obtain converged results for low values of Ca

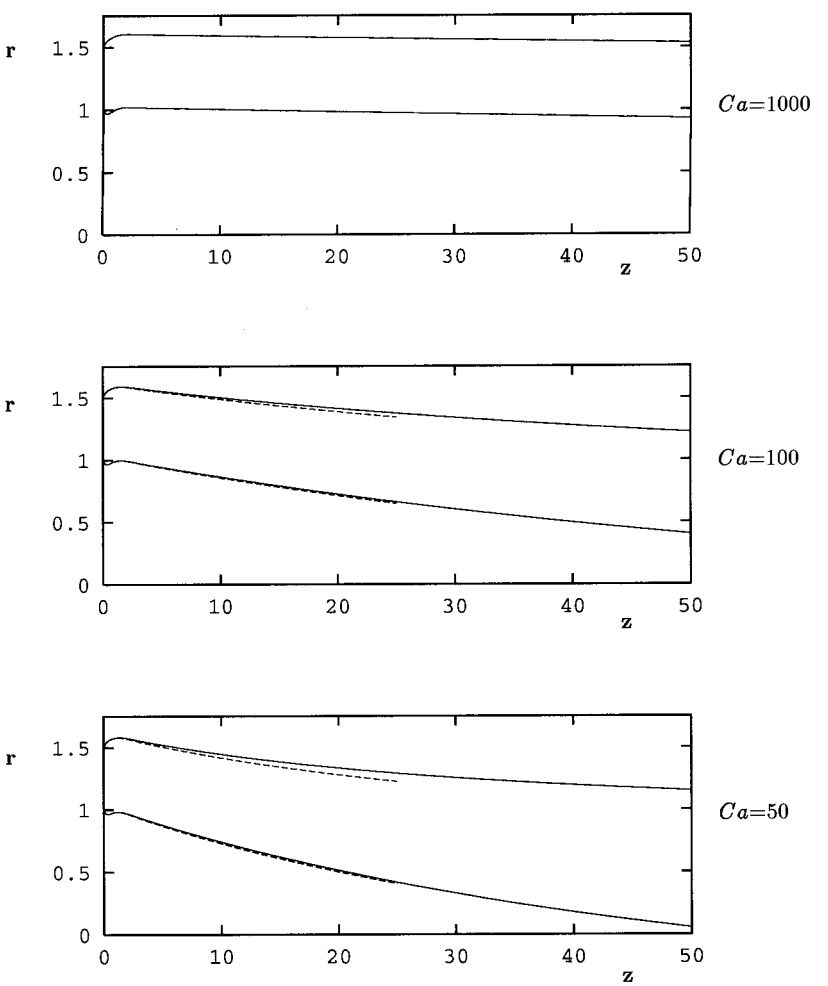

Figure 5. Annular extrudates for various capillary numbers, $\epsilon = 0.5$, $Re = 0$ and $St = \infty$, obtained with $L_2 = 50$ (solid lines) and 25 (dashed lines).

owing to the fact that we are restricted to using rather short solution domains. However, satisfactory results can be obtained for higher values of the Stokes and Reynolds numbers because the value of L_3 increases considerably with these two numbers. In Figure 6, we show the effect of Ca for $Re = 0$ and $St = 0.004$. It is interesting to note that, in this case, the effect of the domain length on the results becomes less important as the surface tension is increased.

The effects of the gravitational force and of the surface tension become less significant as the Reynolds number is increased. In Figure 7, we show the effect of the Reynolds number on the annular film, in the case of $St = 0.0004$ and $Ca = \infty$. Owing to inertia, the motion of the film towards the axis of symmetry becomes slower as the Reynolds number is increased. For $Re = 2$, the initial asymmetric swelling is observed throughout its converged length and both its inner and outer radii are larger than the corresponding ones of the die. In the same case, after the usual initial swelling, the film thickness remains almost constant.

The case of $\epsilon = 0.1$ was examined next. Reducing ϵ from 0.5 to 0.1 decreases the thickness of the film by a factor of 5. This decrease removes the possibility of a short closing length and allows the examination of increased Stokes numbers. The changes of the annular film shapes with the dimensionless numbers of interest are more pronounced and even longer meshes must be employed. In Figure 8(a), we show the annular films obtained with different Stokes numbers in the case of zero Reynolds number and zero surface tension. Note that meshes with L_2 as long as 640 had to be used. In Figure 9(a), we show the effect of the capillary number

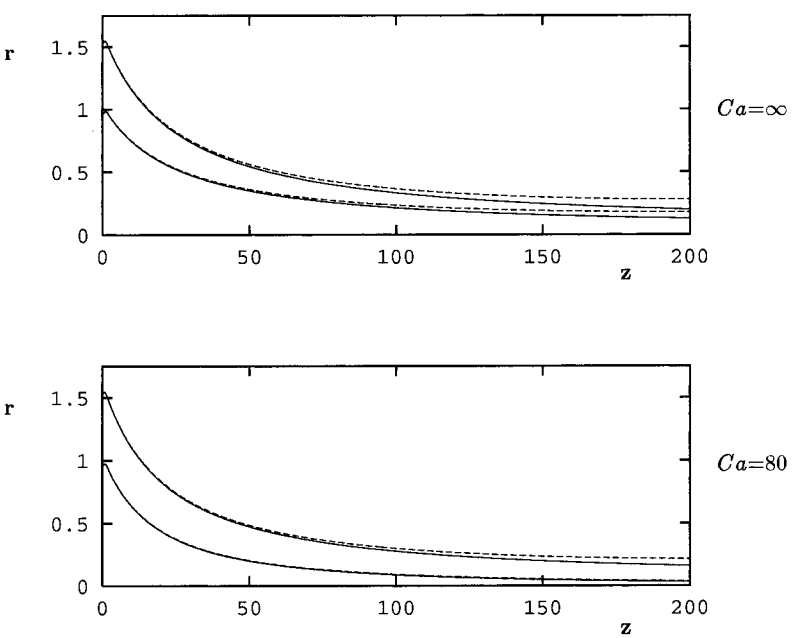

Figure 6. Effect of capillary number on the annular extrudates for $St = 0.004$, $\epsilon = 0.5$ and $Re = 0$ with $L_2 = 400$ (solid lines) and 200 (dashed lines).

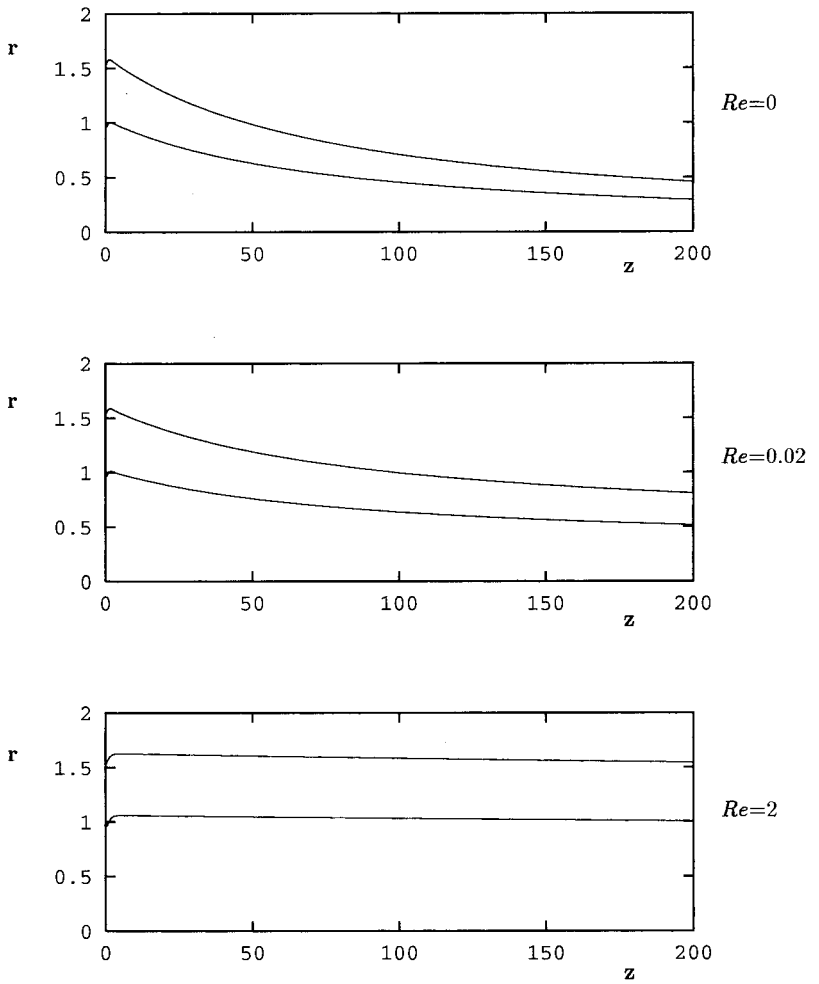

Figure 7. Annular extrudates for $\epsilon = 0.5$, $St = 0.0004$, $Ca = \infty$ and various Reynolds numbers, obtained with a long mesh ($L_2 = 1600$).

by plotting the annular films obtained for $Ca = \infty$ and 200, in the case of $St = 0.01$ and $Re = 0$. The effect of the Reynolds number for zero and non-zero Stokes numbers is illustrated in Figures 10(a) and 11(a) respectively. Note that at high values of the Reynolds number, the annular film is initially pushed far from the axis of symmetry, but gravity eventually prevails further downstream.

The calculations for $\epsilon = 0.1$ were repeated using the one-dimensional model of Section 3. Comparisons of the predictions of the two models are made in Figures 8–11, where it is seen that their results are in qualitative agreement. The only exception is that the one-dimensional

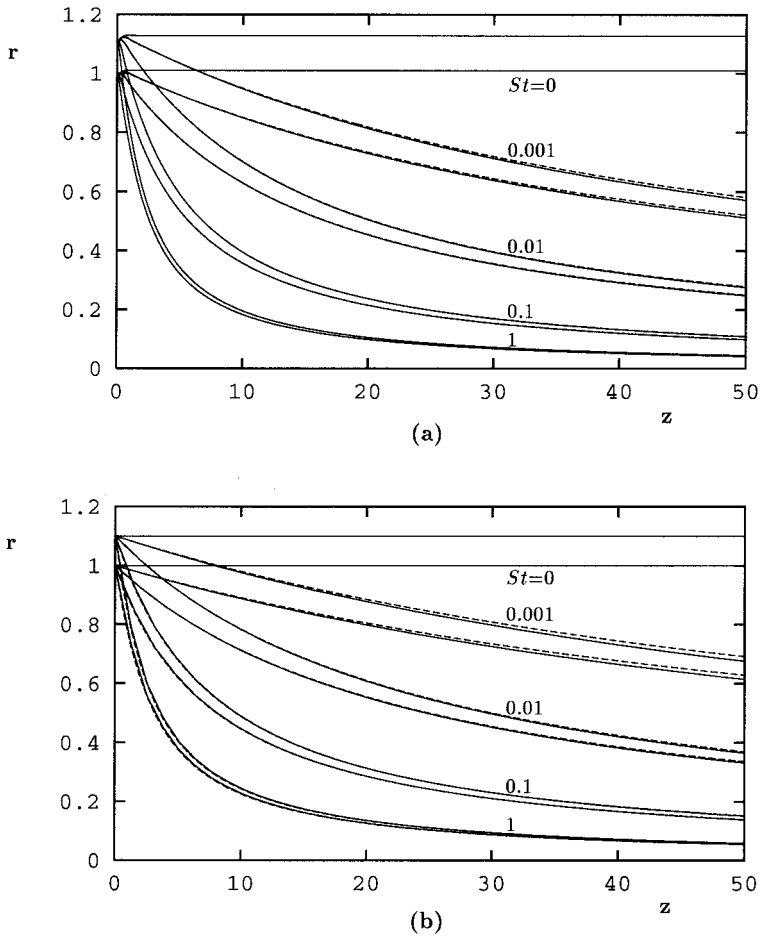

Figure 8. (a) Annular extrudates for $\epsilon = 0.1$, $Re = 0$, $Ca = \infty$ and various Stokes numbers, obtained with $L_2 = 640$ (solid lines) and 320 (dashed lines); (b) one-dimensional predictions.

model predicts a film of constant thickness for all Reynolds numbers when $St = 0$ and $Ca = \infty$ (Figures 8(b) and 10(b)). This should have been expected, since this model does not account for the asymmetric swelling caused by the sharp change of boundary conditions at the die exit and this is the only effect present when $St = 0$ and $Ca = \infty$. Quantitative comparison between the two models can be made by introducing the following definition for the error in results of the one-dimensional model based on the results of the two-dimensional model:

$$E = 100\left|\frac{f_{2D}(z) - f_{1D}(z)}{f_{2D}(z)}\right|, \quad f = h_{in}, h_{out}$$

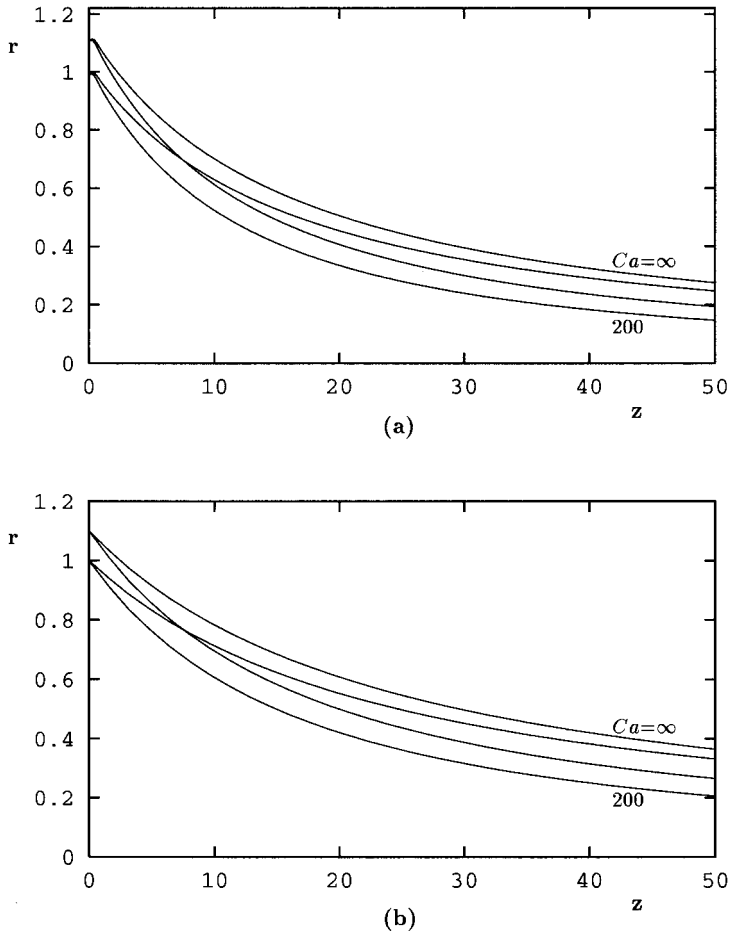

Figure 9. (a) Effect of Ca on the annular extrudates for $\epsilon = 0.1$, $St = 0.01$, $Re = 0$ and $L_2 = 640$; (b) one-dimensional predictions.

Then, from Figures 8–11, we deduce that the maximum error is less than 30 per cent and it occurs at the smallest non-zero value of the Stokes number.

Evidently, the quantitative differences between the predictions of the two models, observed in Figures 8–11, are mostly due to the fact that the one-dimensional model is not valid near the die exit, where the flow is two-dimensional. In the region just outside the die exit, the radial velocity of the inner surface of the film has an even opposite sign from the corresponding velocity of the outer surface. Clearly, the one-dimensional model, which can allow only uniform velocity at the entrance plane and predicts uniform velocity at every cross-section at lowest order, is not able to describe such a flow field. Besides, this was the reason that the

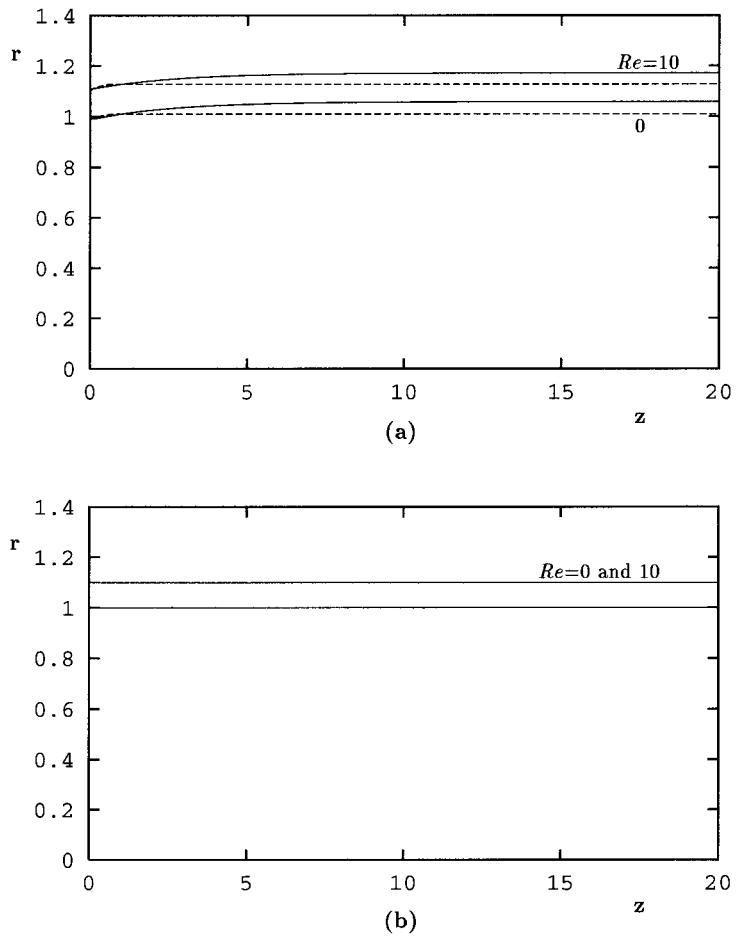

Figure 10. (a) Annular extrudates for $Re = 0$ (dashed lines) and 10 (solid lines), $\epsilon = 0.1$, $St = 0$, $Ca = \infty$ and $L_2 = 640$; (b) one-dimensional predictions.

centre of the co-ordinate system for the one-dimensional model was located at a distance $L_2 - L_4$ (> 0) from the die exit. On the other hand, this shifting, if done arbitrarily as in Figures 8(b)–11(b), introduces additional reasons for deviation between the two sets of results. This is because gravity will accelerate the fluid, and thus increase its axial velocity (even inside the die) and modify its thickness and inner radius from the plane at $z = L_1$ in the two-dimensional model to the plane at $z = 0$ in the one-dimensional model (see Figure 1). These changes in turn will generate small but non-negligible deviations in the characteristic variables used in defining the dimensionless numbers in the two models.

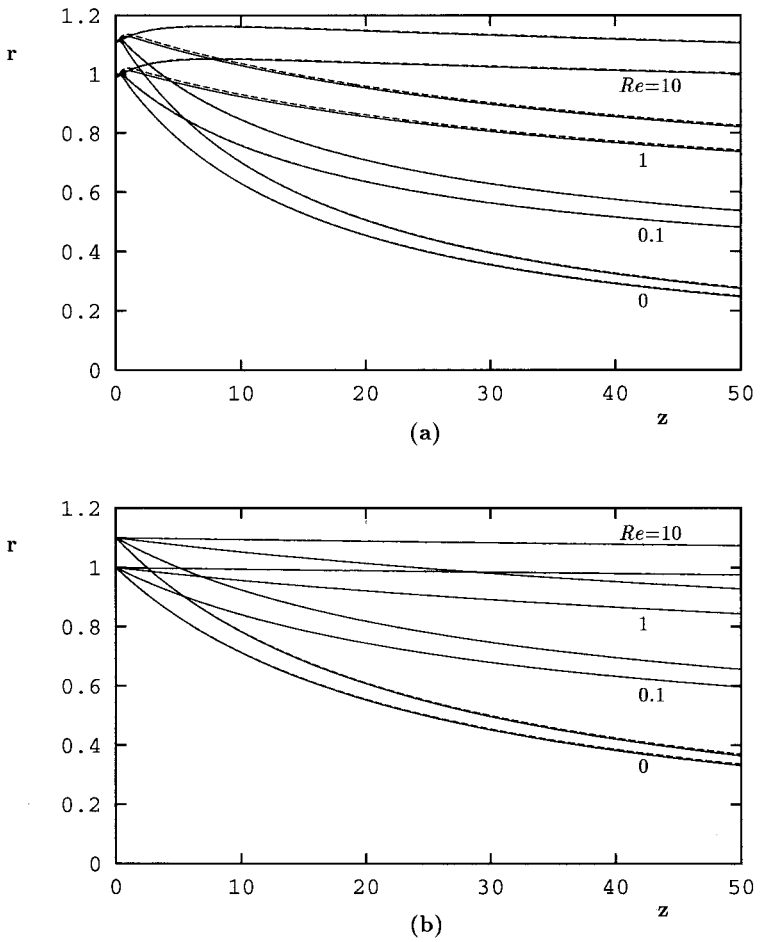

Figure 11. (a) Effect of Re on the annular extrudates for $\epsilon = 0.1$, $St = 0.01$, $Ca = \infty$, obtained with $L_2 = 640$ (solid lines) and 320 (dashed lines); (b) one-dimensional predictions.

Therefore, in order to carry out a fair comparison between the two models, we have to properly account for the length at which the swelling ends and the flow becomes nearly one-dimensional. To this end, the location $z = 0$ in the one-dimensional model should not be set arbitrarily, but it should be at the point where the flow becomes nearly one-dimensional or at the point of maximum swelling of the outer surface. This point is easier to observe experimentally (see Reference [21]). Given the distance of that location from the exit of the die, one would need, in addition, the radius of the inner or the outer surface, the film thickness and the average axial velocity at the point in question. In order to improve the one-dimensional analysis, we will obtain these values from the two-dimensional results and modify accordingly

Table II. Modified parameters for the one-dimensional calculations in Figures 12 and 13 ($Re = 0$ in all cases).

Original values in Figure 8				Modified values in Figure 12			
ϵ	L_2-L_4	Ca	St	ϵ	L_2-L_4	Ca	St
0.1	0	∞	0.001	0.1162	0.5326	∞	0.00120
0.1	0	∞	0.01	0.1166	0.2688	∞	0.01161
0.1	0	∞	0.1	0.1164	0.0786	∞	0.11348
0.1	0	∞	1.0	0.1094	0.0342	∞	1.07283
Original values in Figure 9				Modified values in Figure 13			
ϵ	L_2-L_4	Ca	St	ϵ	L_2-L_4	Ca	St
0.1	0	∞	0.01	0.1166	0.2688	∞	0.01161
0.1	0	200	0.01	0.1191	0.1410	169.05	0.01165

the dimensionless numbers to be used in the one-dimensional simulations. The modified dimensionless numbers are shown in Table II.

In Figures 12 and 13, we compare directly the new one-dimensional predictions to those of the two-dimensional model. Clearly, the agreement between the two sets of results is now much better than in Figures 8 and 9. The maximum error in both cases is about 12 per cent and it still occurs for the smallest non-zero value of St. A similar comparison was made for $\epsilon = 0.5$ between the one- and the two-dimensional models after adjusting the dimensionless numbers

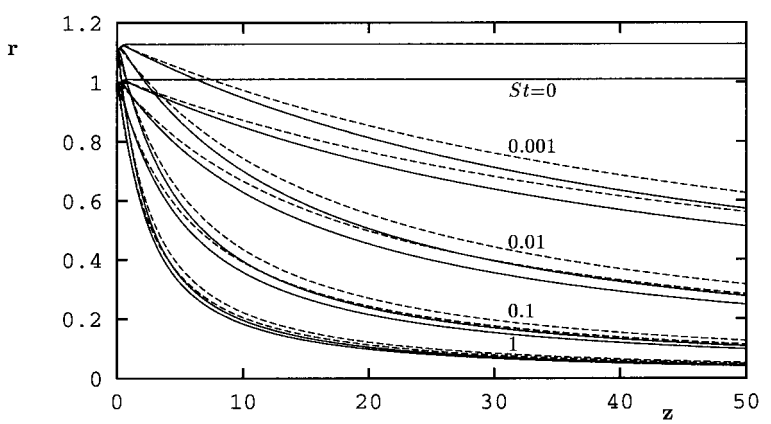

Figure 12. Comparison of the predictions of the two-dimensional model (solid curves) and the one-dimensional model (dashed curves) for $\epsilon = 0.1$, $Re = 0$, $Ca = \infty$, $L_2 = 640$ and various Stokes numbers. One-dimensional calculations start at the point where the outer free surface attains its maximum value in the two-dimensional calculations.

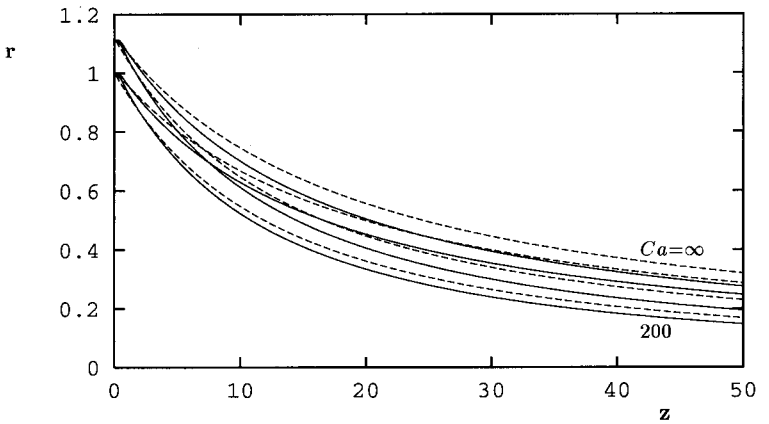

Figure 13. Comparison of the predictions of the two-dimensional model (solid curves) and the one-dimensional model (dashed curves) for $\epsilon = 0.1$, $Re = 0$, $St = 0.01$, $L_2 = 640$ and two values of the capillary numbers. One-dimensional calculations start at the point where the outer free surface attains its maximum value in the two-dimensional calculations.

of the former as described above. The simulations were carried out under the parameter values of Figure 4. It was found that, in spite of the very large value of ϵ, the maximum error was less than 8 per cent. The consistent decrease in the error between the two models with increasing St is due to the fact that the swelling of the fluid decreases as St increases. Therefore, the characteristic values used in determining the dimensionless numbers in the two models get closer together.

Finally, it is noteworthy that the difference in computational cost between the two models is very large. Therefore, one would carry out a few two-dimensional simulations to generate empirical laws for predicting the amount of swelling and where it reaches its maximum as a function of the relevant dimensionless numbers. Then, these dimensionless numbers could be modified as described above and used in the one-dimensional model for a much larger variety of conditions and parameter values to get additional predictions without any appreciable computational cost.

5. CONCLUSIONS

Finite elements have been used to solve the Newtonian annular extrusion problem under gravity and surface tension. Results have been obtained for different Reynolds, Stokes and capillary numbers, and their effects on the shape of the annular film have been investigated for $\epsilon = 0.5$ and 0.1, ϵ being the ratio of the die gap to its inner radius. A one-dimensional model for thin annular films has also been presented. Its predictions agree very well with the two-dimensional calculations, when the distance from the die exit to the maximum swelling is properly accounted for. A comparison between the one-dimensional modelling of steady and

unsteady extrusion [13,14] shows that the Reynolds and capillary numbers affect the film in a similar way. In contrast, gravity affects annular extruded films in a qualitatively different way. In steady extrusion, the film moves monotonically towards the axis of symmetry, whereas in unsteady extrusion, its radius exhibits a minimum at about half its length. Of course, simulations of two-dimensional unsteady extrusion are much more difficult to model and compute numerically.

ACKNOWLEDGMENTS

This work was partially supported under the PENED-95 Program (Grant number 58, Section 1.3) of the General Secretariat of Research and Technology of Greece.

REFERENCES

1. Crochet MJ, Keunings R. Die swell of a Maxwell fluid: numerical prediction. *Journal of Non-Newtonian Fluid Mechanics* 1980; **7**: 199–212.
2. Mitsoulis E. Extrudate swell of Newtonian fluids from annular dies. *AIChE Journal* 1986; **32**: 497–500.
3. Mitsoulis E, Heng FL. Extrudate swell of Newtonian fluids from converging and diverging annular dies. *Rheologica* 1987; **26**: 414–417.
4. Ahn Y-C, Ryan ME. Analysis of extrudate swell from an annular die. *Computers & Fluids* 1992; **21**: 267–289.
5. Huynh BP. A numerical investigation of non-isothermal extrusion through annular dies. *International Journal of Engineering Science* 1998; **36**: 171–188.
6. Garcia-Rejon A, DiRaddo RW, Ryan ME. Effect of die geometry and flow characteristics on viscoelastic annular swell. *Journal of Non-Newtonian Fluid Mechanics* 1995; **60**: 107–128.
7. Dutta A, Ryan ME. Dynamics of a creeping Newtonian jet with gravity and surface tension: a finite difference technique for solving steady free-surface flows using orthogonal curvilinear coordinates. *AIChE Journal* 1982; **28**: 220–232.
8. Finnicum DS, Weinstein SJ, Ruschak KJ. The effect of applied pressure on the shape of a two-dimensional liquid curtain falling under the influence of gravity. *Journal of Fluid Mechanics* 1993; **255**: 647–665.
9. Georgiou GC, Papanastasiou TC, Wilkes JO. Laminar jets at high Reynolds and high surface tension. *AIChE Journal* 1988; **24**(9): 1559–1562.
10. De Luca L, Costa M. Two-dimensional flow of a liquid sheet under gravity. *Computers & Fluids* 1995; **24**: 401–414.
11. Goodwin RT, Schowalter WR. Arbitrarily oriented capillary-viscous planar jets in the presence of gravity. *Physics of Fluids* 1994; **7**: 954–963.
12. Hassan MZ, Mitsutake Y, Monde M. Shape of an annular liquid jet. *Journal of Fluids and Engineering* 1997; **119**: 591–596.
13. Housiadas K, Tsamopoulos J. Unsteady flow of an axisymmetric annular film under gravity. *Physics of Fluids* 1998; **10**: 2500–2516.
14. Housiadas K, Tsamopoulos J. Unsteady extrusion of a viscoelastic annular film. I: general model and its numerical solution. *Journal of Non-Newtonian Fluid Mechanics* 2000; **88**: 229–259.
15. Housiadas K, Tsamopoulos J. Unsteady extrusion of a viscoelastic annular film. II: linearized model and its analytical solution. *Journal of Non-Newtonian Fluid Mechanics* 2000; **88**: 303–325.
16. Pearson JRA, Petrie CJS. The flow of a tubular film. Part 2: interpretation of the model and discussion of solutions. *Journal of Fluid Mechanics* 1970; **42**: 609–625.
17. Schultz WW, Davis SH. One-dimensional liquid fibers. *Journal of Rheology* 1982; **26**: 331–345.
18. Yarin AL, Gospodinov P, Roussinov VI. Stability loss and sensitivity in hollow fiber drawing. *Physics of Fluids* 1964; **6**: 1454–1463.
19. Pearson JRA, Petrie CJS. The flow of a tubular film. Part 1: Formal mathematical representation. *Journal of Fluid Mechanics* 1970; **40**: 1–19.
20. Trang CT, Yeow YL. Extrudate swell of Newtonian and non-Newtonian fluids. *Journal of Non-Newtonian Fluid Mechanics* 1986; **20**: 103–116.
21. Beris AN, Liu B. Time-dependent fiber spinning equations. 1. Analysis of the mathematical behavior. *Journal of Non-Newtonian Fluid Mechanics* 1988; **26**: 341–361.

